Japanese Journal of Applied Physics

The Japan Society of Applied Physics

RAPID COMMUNICATION

# Magnetotransport of thin film $Sr_{1-x}La_xCuO_2$ on (110) $DyScO_3$

To cite this article: Jana Lustikova *et al* 2022 *Jpn. J. Appl. Phys.* **61** 040904

View the article online for updates and enhancements.

You may also like

- Memory characteristics and the tunneling mechanism of Au nanocrystals embedded in a $DyScO_3$ high-*k* gate dielectric layer
K C Chan, P F Lee, D F Li et al.
- Temperature dependence on the domain structure of epitaxial $PbTiO_3$ films grown on single crystal substrates with different lattice parameters
Yoshitaka Ehara, Takaaki Nakashima, Daichi Ichinose et al.
- Refractive index and interband transitions in strain modified $NaNbO_3$ thin films grown by MOCVD
S Bin Anooz, P Petrik, M Schmidbauer et al.

This content was downloaded from IP address 128.210.107.131 on 30/03/2022 at 22:31

Japanese Journal of Applied Physics **61**, 040904 (2022) **RAPID COMMUNICATION**
https://doi.org/**10.35848/1347-4065/ac50bc**

# Magnetotransport of thin film $Sr_{1-x}La_xCuO_2$ on (110) $DyScO_3$

Jana Lustikova[1,2*], Rui-Feng Wang[3], Yong Zhong[3], ShuZe Wang[3], Akichika Kumatani[1,2,4,5], Xu-Cun Ma[3,6], Qi-Kun Xue[3,6,7,10], and Yong P. Chen[1,2,8,9,11]

[1]*Center for Science and Innovation in Spintronics, Tohoku University, Sendai 980-8577, Japan*
[2]*Advanced Institute for Materials Research (WPI-AIMR), Tohoku University, Sendai 980-8577, Japan*
[3]*State Key Laboratory of Low-Dimensional Quantum Physics, Department of Physics, Tsinghua University, Beijing 100084, People's Republic of China*
[4]*Graduate School of Environmental Studies, Tohoku University, Sendai 980-856, Japan*
[5]*International Center for Materials Nanoarchitectonics (WPI-MANA), National Institute for Materials Science (NIMS), Namiki 1-1, Tsukuba, Ibaraki 305-0044, Japan*
[6]*Frontier Science Center for Quantum Information, Beijing 100084, People's Republic of China*
[7]*Beijing Academy of Quantum Information Sciences, Beijing 100193, People's Republic of China*
[8]*Purdue Quantum Science and Engineering Institute, and Department of Physics and Astronomy, Purdue University, West Lafayette, IN 47907, United States of America*
[9]*School of Electrical and Computer Engineering, and Birck Nanotechnology Center, Purdue University, West Lafayette, IN 47907, United States of America*
[10]*Southern University of Science and Technology, Shenzhen 518055, People's Republic of China*
[11]*Institute of Physics and Astronomy and Villum Center for Hybrid Quantum Materials and Devices, Aarhus University, 8000 Aarhus-C, Denmark*

*E-mail: lustikova@tohoku.ac.jp

Received November 10, 2021; revised December 30, 2021; accepted January 31, 2022; published online March 17, 2022

We report measurements of low-temperature magnetoresistance in $Sr_{1-x}La_xCuO_2$ ($x = 0.1$) epitaxial thin film grown on (110) $DyScO_3$ single crystal. A positive magnetoresistance which is anisotropic and hysteretic with respect to the in-plane direction of magnetic field appears in $Sr_{1-x}La_xCuO_2$ below $T = 5$ K, coinciding with antiferromagnetic ordering and strong magnetic anisotropy in $DyScO_3$. The interplay of magnetotransport in epitaxial $Sr_{1-x}La_xCuO_2$ with magnetism in the substrate is discussed based on magnetostriction and magnetic relaxation in $DyScO_3$. © 2022 The Japan Society of Applied Physics

Supplementary material for this article is available online

The infinite-layer (IL) compounds $Sr_{1-x}Ln_xCuO_2$ (Ln = La, Sm, Nd, etc.) offer a unique opportunity to explore the fundamental properties of high-temperature cuprates as their crystal structure is composed solely of $CuO_2$ planes alternated by Sr (Ln) planes.[1–9] Yet they have not been studied as extensively as other families of cuprates, e.g. $R_2CuO_4$ (R = La, Nd) compounds.[10] One of the reasons lies in the experimental difficulty of growing bulk single crystals through high-pressure synthesis.[11–13] However, growth of single crystal thin films in the IL phase is possible owing to the epitaxial effect.[14] The resistivity and $T_c$ of $Sr_{1-x}La_xCuO_2$ thin films vary significantly depending both on the doping level and on the lattice constant of the substrate.[14–20] The highest $T_c$ over 40 K is achieved at La content $x = 0.1$ on (110) $DyScO_3$ substrates which optimize lattice constant matching and can provide essentially strain free $Sr_{1-x}La_xCuO_2$ films.[21]

Although the rare-earth perovskite $DyScO_3$ has been increasingly used as a substrate for epitaxial growth of cuprate or perovskite films,[16,21–24,8] the interplay between the electronic properties in epitaxial thin films and the magnetism in $DyScO_3$ remains largely unexplored. $DyScO_3$ hosts a large paramagnetic moment facilitated by Dy moments, large magnetic anisotropy and a Néel transition at 3.1 K.[25–30] The large paramagnetic moment of $DyScO_3$ at low temperatures was shown to induce thermal spin injection into Pt films,[29] and recently unconventional low-temperature magnetoresistance was reported in epitaxial $SrIrO_3$ films on (110) $DyScO_3$.[31]

Magnetic substrate effects on transport in thin films are especially interesting from the perspective of spintronics[32] which seeks to exploit the interplay of electronic spin and charge degrees of freedom in a variety of systems.[33,34] In this stream, it is highly attractive to explore how magnetism of the substrate can affect transport phenomena in high-Tc cuprate films and to gain insights into the interplay of magnetism and electronic transport properties in these materials.[5,35,36] In this work, we study the low-temperature magnetoresistance in infinite-layer $Sr_{1-x}La_xCuO_2$ ($x = 0.1$) thin films epitaxially grown on $DyScO_3$. We find anisotropic magnetoresistance and hysteretic angular magnetoresistance which coincide with magnetic anisotropy and magnetic phase transitions in $DyScO_3$. The absence of such features in Cu and Pt polycrystalline reference films indicates a much larger influence of $DyScO_3$ substrate on magnetotransport in epitaxial $Sr_{1-x}La_xCuO_2$.

For this study, $c$-axis oriented epitaxial $Sr_{1-x}La_xCuO_2$ ($x = 0.1$) films with a thickness of 20 nm were grown on $DyScO_3$ (110) substrates by ozone-assisted molecular beam epitaxy (MBE) as detailed elsewhere.[7,8] The $c$-axis of $Sr_{1-x}La_xCuO_2$ is perpendicular to the substrate. The lattice constants for the $DyScO_3$ (110) face, $\sqrt{(a^2 + b^2)}/2 = 3.944$ Å and $c_0/2 = 3.943$ Å, coincide very closely with each other and provide very good lattice matching for $Sr_{0.9}La_{0.1}CuO_2$ (bulk $a_0 = 3.949$ Å).[21] $DyScO_3$ substrates were purchased from MTI Corporation. Orientation of crystal axes in $DyScO_3$ substrates was confirmed by Laue diffraction. $DyScO_3$ is a good insulator with a band gap of 5.9 eV.[25] Field- and temperature-dependent magnetization of the $DyScO_3$ substrates were measured using the vibrating sample magnetometry (VSM) option of the physical property measurement system (PPMS; Quantum Design) by fixing the samples on quartz holders with varnish GE7031. The size of the substrates was 2 mm × 10 mm with a thickness of 0.5 mm. $Sr_{1-x}La_xCuO_2$ covered an area of 2 mm × 6 mm in the center of the substrate. The conventional four-terminal measurement was implemented to measure the magnetoresistance in $Sr_{1-x}La_xCuO_2$ using the PPMS system, where the temperature was decreased down to 2 K. Electric contacts were made by pressing golden wires coated in indium into the $Sr_{1-x}La_xCuO_2$ film surface. Magnetoresistance was

 © 2022 The Japan Society of Applied Physics

measured by applying a DC electric current of 10 $\mu$A. The direction of the magnetic field was varied by rotating the sample in the magnetic field using a rotating sample holder. Reference films of polycrystalline[37–40] Cu (7 nm) and Pt (5 nm) were grown on identical $DyScO_3$ substrates by magnetron sputtering at room temperature in a Hall bar geometry with a nominal width 0.2 mm and length 1 mm. The growth rates for Cu and Pt were 0.154 nm $s^{-1}$ and 0.146 nm $s^{-1}$, respectively.

The resistivity versus temperature ($\rho$–$T$) curve in a $Sr_{1-x}La_xCuO_2$ film on $DyScO_3$ is shown in Fig. 1(a). The $\rho$–$T$ curve shows a semiconducting behaviour. Although superconductivity with $T_c$ as high as 40 K is expected in $Sr_{1-x}La_xCuO_2$ ($x = 0.1$), semiconducting $\rho$–$T$ curves have been reported in MBE films of similar doping content on (110) $DyScO_3$ and may result from a small quantity of apical oxygen.[41,42] In our case, apical oxygen may get incorporated during air exposure after the sample is transferred out of the high-vacuum environment.

For the $DyScO_3$ substrate, we show the temperature-dependent magnetization ($M$–$T$) in Fig. 1(b), with the magnetic field $H = 1$ kOe applied along the [−110] and [001] directions. Magnetization steeply increases at low temperatures. We observe a maximum in magnetization at 3.1 K corresponding to an antiferromagnetic Néel transition.[30] The magnetization along [−110] direction is 49-times larger than that along [001] with the same applied field at $T = 3$ K, confirming strong magnetic anisotropy.[28,29] The anisotropy axes for the Dy ions are known to be lying in the *ab* plane of the crystal.[30] Therefore, for magnetic fields parallel to the (110) plane of the substrate surface, [−110] direction corresponds to an easy axis and [001] to a hard axis. The field-dependent magnetization ($M$–$H$) along [−110] direction in Fig. 1(c) shows linear paramagnetic behaviour for temperatures above 10 K. At $T = 2$ K, shown in Fig. 1(d), $M$–$H$ along [−110] direction is linear at low fields, followed by a steep increase at $H_s \sim 3$ kOe, and then a gentler slope. The increase at $H_s$ and hysteresis signify magnetic transitions from an antiparallel to a canted configuration.[28,30] $M$–$H$ along [001] direction is linear up to 10 kOe with a much smaller magnitude, as expected for a hard axis.

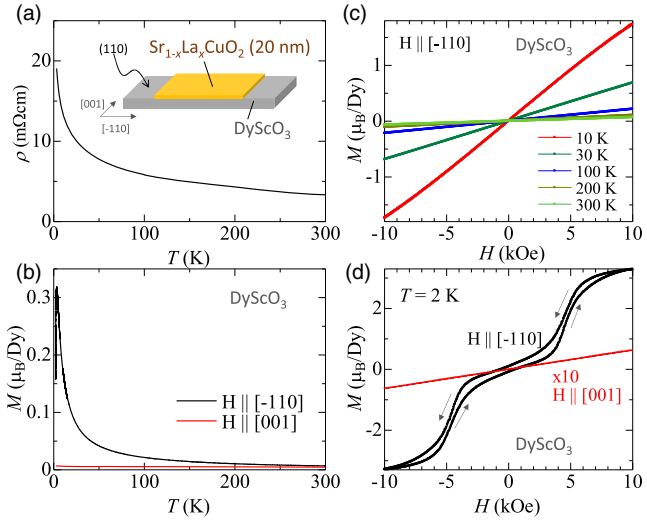


**Fig. 1.** (Color online) Sample characterization. (a) $\rho(T)$ curve of $Sr_{1-x}La_xCuO_2$ (20 nm) epitaxial film grown by molecular beam epitaxy in 001 direction on $DyScO_3$ (110). Inset shows a schematic illustration of the sample. Gray arrows denote crystal axes of $DyScO_3$. (b) Temperature-dependent magnetization of $DyScO_3$ at 1 kOe measured along [−110] and [001] directions. (c) $M$ versus $H$ for $DyScO_3$ along [−110] direction shown at various temperatures. (d) $M$ versus $H$ for $DyScO_3$ at temperature 2 K for magnetic fields along [−110] and [001] directions. Data for [001] are plotted multiplied by a factor of 10 for better visibility.

Figure 2(a) shows the field-sweeps of low-temperature magnetoresistance, $[\rho(H) - \rho_0]/\rho_0$, in $Sr_{1-x}La_xCuO_2$ with magnetic field along $DyScO_3$ [001] direction. Positive magnetoresistance is observed for $T = 2$ K and 5 K, and decreases with increasing temperature. No magnetoresistance could be discerned for all measured temperatures from 10 to 300 K within an accuracy of 0.02%. For comparison, a positive low-temperature magnetoresistance that decreases with increasing temperature and vanishes between 5 and 10 K was also observed in Cu (7 nm) film on $DyScO_3$ [Fig. 2(b)] but was absent in Pt (5 nm) films on $DyScO_3$ [Fig. 2(c)]. The temperature dependence of magnetoresistance ratio at 10 kOe, $[\rho(10\text{kOe}) - \rho_0]/\rho_0$, is shown in Fig. 2(f). The magnetoresistance ratio in $Sr_{1-x}La_xCuO_2$ is at least one order of magnitude larger than that in Cu or Pt, and increases at low-temperature approaching the Néel temperature of $DyScO_3$ [$M$–$T$ curves shown for comparison in Fig. 2(e)].

Field sweeps of magnetoresistance at $T = 2$ K in $Sr_{1-x}La_xCuO_2$ for selected directions $\phi$ of the magnetic field in the $DyScO_3$ (110) plane are shown in Fig. 3(a), where $\phi$ is the in-plane rotation angle between the magnetic field direction and $DyScO_3$ [001] axis. Magnetoresistance is positive for all measured directions. Jumps and hysteretic loops are apparent in the field sweeps, but a repeated measurement shows that these are random and not reproducible (shown for $\phi = 25°$). We assume that these are related to the quality of electric contacts to the sample which has kΩ resistance. Figure 3(b) shows a polar plot of the magnetoresistance ratio $[\rho(10\text{kOe}) - \rho_0]/\rho_0$ versus $\phi$ for both $Sr_{1-x}La_xCuO_2$ and Cu. The magnetoresistance ratio in $Sr_{1-x}La_xCuO_2$ is $0.25 \pm 0.05\%$ for $\phi = 0°$ and $0.35 \pm 0.05\%$ for $\phi = 90°$. For comparison, the magnetoresistance ratio in Cu is $0.030 \pm 0.003$ for $\phi = 0°$ and $0.028 \pm 0.003$ for $\phi = 90°$. Thus, the magnetoresistance ratio in $Sr_{1-x}La_xCuO_2$ is anisotropic in the $DyScO_3$ (110) plane with a slight increase for $DyScO_3$ [−110] direction ($\phi = 90°$, easy axis) compared to [001] ($\phi = 0°$, hard axis). By contrast, no anisotropy is seen in Cu or Pt.

Figure 4 shows a measurement of the angular magnetoresistance, $[\rho(\phi) - \rho_0]/\rho_0$, where a magnetic field of fixed strength is rotated in the (110) plane of $DyScO_3$. Each point is measured by first rotating the magnetic field of fixed strength from the previous measured angle to the current angle $\phi$, waiting for a delay $\tau = 1$ s, and then recording the resistance. As the magnetic field is rotated between the hard and easy axes of $DyScO_3$, a two-fold angular magnetoresistance with sharp peaks and dips is observed at $T = 2$ K and $H = 10$ kOe and gradually smooths out for 5 kOe, 2 kOe [Fig. 4(a)]. A 10-times smaller angular magnetoresistance is observed at $T = 5$ K, and no angular magnetoresistance could be discerned at $T = 10$ K [Fig. 4(b)]. Significantly, when the sense of rotation is reversed, a hysteresis is observed [Fig. 4(c)]. For comparison, neither Cu [Fig. 4(d)] nor Pt [Fig. 4(e)] films on $DyScO_3$ show such oscillations. We note that oscillations and hysteresis in $Sr_{1-x}La_xCuO_2$ angular magnetoresistance are observed at such temperatures and


© 2022 The Japan Society of Applied Physics

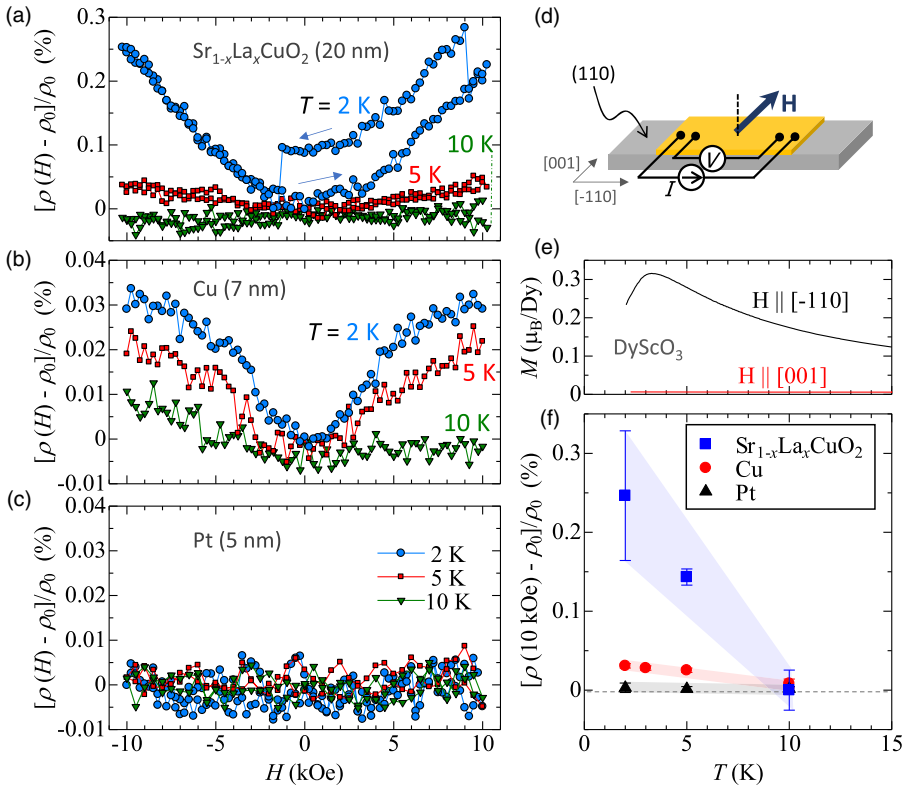


**Fig. 2.** (Color online) Low-temperature magnetoresistance in $Sr_{1-x}La_xCuO_2$ and plain metallic thin films on $DyScO_3$. Normalized magnetoresistance as a function of magnetic field shown for temperatures $T = 2$, 5, 10 K for (a) $Sr_{1-x}La_xCuO_2$ (20 nm), (b) Cu (7 nm), (c) Pt (5 nm). (d) Schematic illustration of the measurement setup. The magnetic field is fixed along $DyScO_3$ [001] direction and current (10 $\mu$A) flows along [−110] direction. $\rho_0$ is the resistivity at 0 kOe. (e) Close up on $DyScO_3$ $M$–$T$ curves for [−110] and [001] directions at low-temperature. (f) Temperature dependence of normalized magnetoresistance at $H = 10$ kOe for $Sr_{1-x}La_xCuO_2$, Cu and Pt. Thick shadow lines are guides for the eyes.

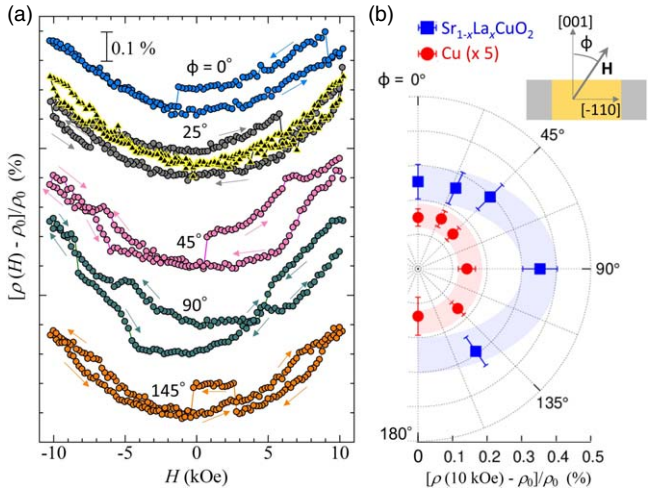


**Fig. 3.** (Color online) Magnetoresistance in $Sr_{1-x}La_xCuO_2/DyScO_3$ at $T =$ 2 K for various directions of magnetic field in the (110) plane of $DyScO_3$. (a) Normalized magnetoresistance as a function of magnetic field shown for angles $\phi = 0$, 25, 45, 90, and 145° between [001] direction of $DyScO_3$ and magnetic field. Magnetoresistance curves are offset for improved visibility. Data for $\phi = 25°$ are shown for two separate measurements (grey dots and black triangles with yellow borders). (b) Polar plot of normalized magnetoresistance ratio at $H = 10$ kOe versus $\phi$ for $Sr_{1-x}La_xCuO_2$ and Cu. Error bars correspond to the size of hysteresis and magnetoresistance jumps in field-sweeps. Data for Cu are plotted multiplied by a factor of 5 for enhanced visibility. Blue and red shadows are guides for the eyes. Inset shows the definition of $\phi$.

magnetic fields where a rotation between $DyScO_3$ [001] ($\phi = 0°$) and [−110] ($\phi = 90°$) directions corresponds to a transition from an antiparallel to a canted configuration of Dy magnetic moments in $DyScO_3$. At $T = 2$ K and $H = 10$ kOe, where we observed the most significant oscillations in angular magnetoresistance, the $M$–$H$ curve in Fig. 1(d) for [001] is linear, while a metamagnetic transition occurred for [−110] at $H_s \sim 3$ kOe. By contrast, the angular magnetoresistance is largely flattened at 2 kOe $< H_s$, where $M$–$H$ for both [001] and [−110] are in a linear region. This is also the case in the absence of oscillations for temperatures 10 K or higher [Fig.1(c)].

The observation of positive magnetoresistance in $Sr_{1-x}La_xCuO_2$ at temperatures and fields coinciding with magnetic ordering in $DyScO_3$ strongly suggests a substrate-induced mechanism. Large magnetic moments in the substrate can affect transport properties of thin films by spin injection or spin Hall magnetoresistance effects.[43,29] However, magnetoresistance effects in both Cu and Pt reference films on $DyScO_3$, which are weak and strong spin-to-charge converters, respectively,[43] were largely absent. This makes an interface spin accumulation mechanism unlikely. As the strong magnetocrystalline anisotropy in $DyScO_3$ is known to cause the substrates to physically crack[28] in magnetic fields of a few 10 kOe, we consider magnetostriction induced strain as a possible origin.[44,45] Since Cu and Pt are polycrystalline films and simple metals with dense carriers, they could be less affected by substrate magnetostriction than epitaxial $Sr_{1-x}La_xCuO_2$.

$DyScO_3$ magnetostriction along [−110] was measured with a chromium film strain gage sputtered directly on $DyScO_3$ (Ref. 46; see also supplemental data and Fig. S1


© 2022 The Japan Society of Applied Physics

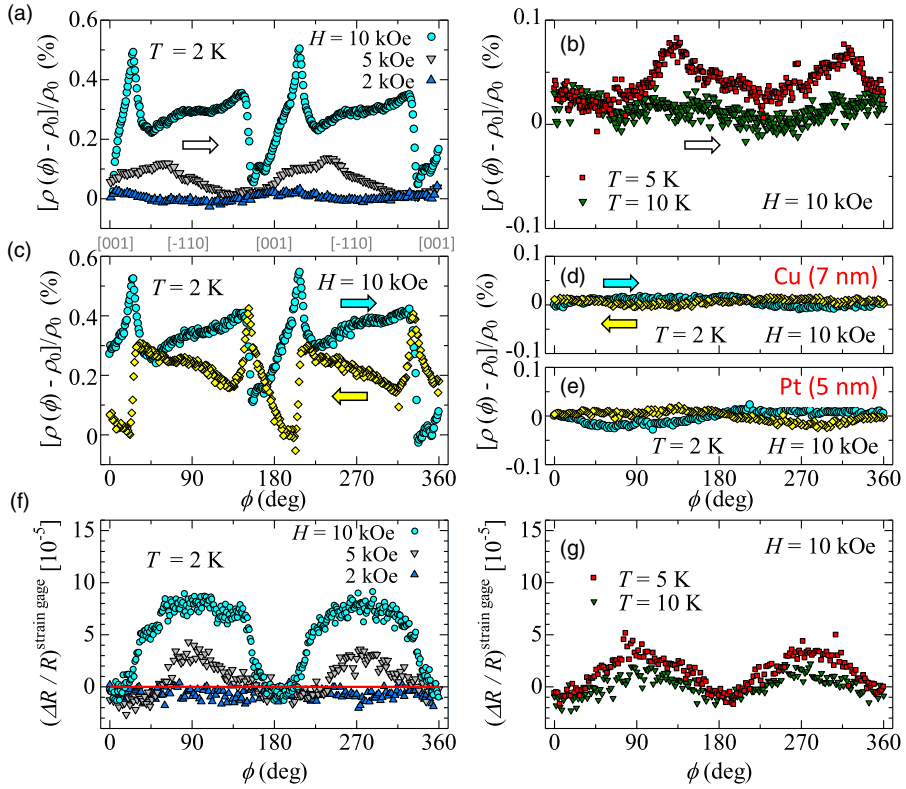


**Fig. 4.** (Color online) Oscillations of the isothermal normalized angular magnetoresistance in $Sr_{1-x}La_xCuO_2/DyScO_3$ and magnetostriction in $DyScO_3$. Normalized angular magnetoresistance in $Sr_{1-x}La_xCuO_2$ for $H = 10$ kOe, 5 kOe, and 2 kOe at (a) $T = 2$ K, and for (b) $H = 10$ kOe, at $T = 5$ K, 10 K. $\phi$ is the angle between [001] direction and the magnetic field vector in the (110) plane of $DyScO_3$. Hysteresis of angular magnetoresistance with respect to sense of magnetic field rotation in (c) $Sr_{1-x}La_xCuO_2$, (d) Cu, and (e) Pt at $H = 10$ kOe, $T = 2$ K. Blue circles and yellow diamonds denote clockwise and anti-clockwise rotation of magnetic field, respectively. Upper axis labels in (c) show the $DyScO_3$ crystal axes corresponding to each direction of magnetic field. Angular dependence of strain response in a film strain gage on $DyScO_3$ for (f) $H = 10$, 5, 2 kOe at $T = 2$ K, and (g) for $H = 10$ kOe at $T = 5$, 10 K. Zero strain is visualized by a red line in (f).

available online at stacks.iop.org/JJAP/61/040904/mmedia for extraction of strain response). Figure 4(f) shows the strain-related change in the gage resistance $(\Delta R/R)^{\text{strain gage}}$ for rotations in magnetic fields $H = 10$, 5, 2 kOe at $T = 2$ K. A negative strain is observed for fields along hard axis [001] ($\phi = 0$, 180°). In $H = 10$ kOe, the strain reverses to positive values at $\phi \sim 17°$, then abruptly increases, and reaches a broad maximum around [−110] easy axis ($\phi \sim 34°$ to 145°). Another sign reversal is observed approaching [001] direction at $\phi \sim 170°$. Using a typical gage factor $GF = (\Delta R/R)^{\text{straingage}}/\epsilon \sim 10$ for chromium film gauges prepared under similar conditions,[47] we obtain a strain $\epsilon \sim +8.0 \times 10^{-6}$ for $H||[-110]$ and $\epsilon \sim -0.5 \times 10^{-6}$ for $H||[001]$ at $T = 2$ K, $H = 10$ kOe. Both the magnitudes and the sign reversal are comparable with magnetostriction reported in a related compound $DyAlO_3$.[44,45] The two-fold symmetry of the angular magnetostriction agrees with the two-fold symmetry of the angular magnetoresistance. Further, $\phi$ intervals of abrupt increase (decrease) in magnetostriction correspond to $\phi$ intervals where sharp magnetoresistance peaks (dips) are observed (see also supplemental data, Fig. S2). Angle intervals of gradual change in magnetoresistance coincide with angle intervals of magnetostriction maxima. At lower fields, the angular change in strain is less abrupt or largely absent [$H = 5$ kOe and 2 kOe in Fig. 4(f)], which is also in agreement with the smoothing of angular magnetoresistance at lower fields in Fig. 4(a). In addition, Fig. 4(g) shows that the angular change of strain at increased temperatures $T = 5$, 10 K is smoother and less than 50% of that at $T = 2$ K, in correspondence with angular magnetoresistance in Fig. 4 (b).

We examine the angular magnetoresistance in $Sr_{1-x}La_xCuO_2$ by changing the delay time $\tau$ between the rotation of magnetic field and the recording of resistance. Figure 5(a) shows the angular magnetoresistance measured by the same protocol as in Fig. 4, by first rotating a magnetic field of fixed strength from the previous measurement point to the current measurement point $\phi$, waiting for a delay $\tau = 1$ s, and then recording the resistance. By increasing $\tau$ to 2 s, the hysteretic peaks become less pronounced [Fig. 5(b)] and eventually vanish for $\tau = 5$, 10 s [Figs. 4(c), 4(d)]. This indicates a transient character of the oscillations and hysteresis in angular magnetoresistance. In spite of the correspondence between the angular magnetoresistance and the angular change in $DyScO_3$ magnetostriction at $\tau = 1$ s in Figs. 4(c), 4(f), the latter shows only a weak hysteresis and no significant change in the position and magnitude of strain extrema with increasing $\tau$ (supplemental data, Fig. S3). Therefore, instead of a simple magnetostriction effect from the substrate, we speculate that the time-dependent angular magnetoresistance could be related to reconfigurations of substrate Dy magnetic moments after a rotation in magnetic field.

The time scale of magnetization relaxation in $DyScO_3$ was confirmed by ac susceptibility $\chi_{ac}$ measurements using a Quantum Design MPMS superconducting quantum interference device magnetometer. We plot the frequency dependence


© 2022 The Japan Society of Applied Physics

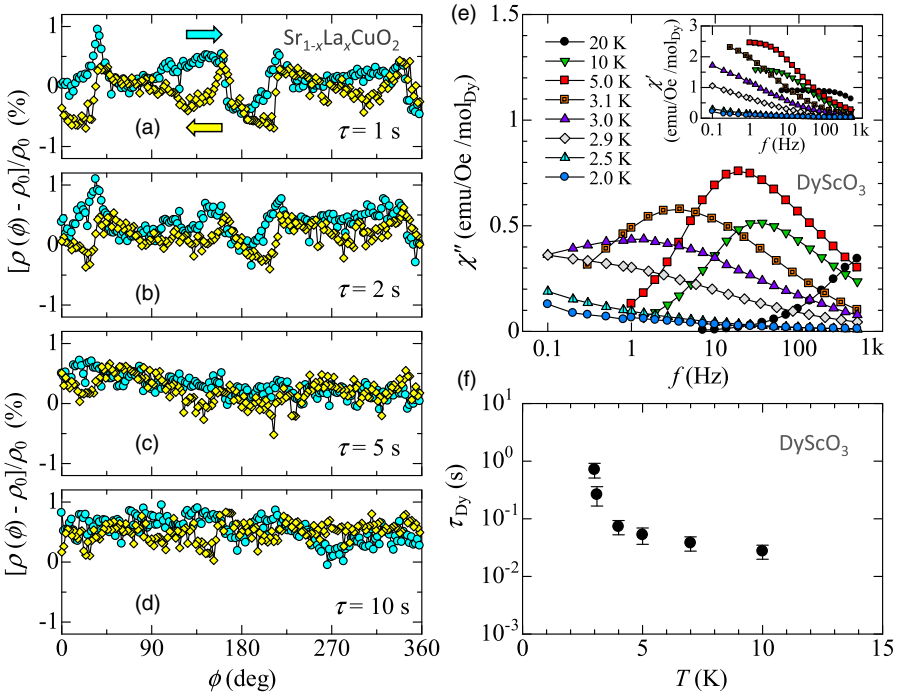


**Fig. 5.** (Color online) Hysteresis in isothermal normalized angular magnetoresistance with respect to the sense of rotation for $Sr_{1-x}La_xCuO_2$ at $H = 10$ kOe, $T = 2$ K for various delay times $\tau$ between magnetic field rotation and resistance data recording, (a) $\tau = 1$ s, (b) $\tau = 2$ s, (c) $\tau = 5$ s, and (d) $\tau = 10$ s. (e) The imaginary part of the $DyScO_3$ ac susceptibility, $\chi''(f)$, as a function of frequency at selected temperatures with ac magnetic field applied along the [−110] direction. The inset shows the real part $\chi'(f)$. (f) The temperature dependence of the characteristic magnetization relaxation time $\tau_{Dy}(T)$ in $DyScO_3$, where $\chi''(f)$ show maxima. The error bars come from the frequency step size.

of the imaginary part of the ac susceptibility $\chi''(f)$ at selected temperatures in Fig. 5(e). The magnitude of the applied ac field along [−110] was 3 Oe. For temperatures from 10 to 3 K, clear maxima are seen in $\chi''(f)$, which move to lower frequency with decreasing temperature. We use the maxima in $\chi''(f)$ to obtain a characteristic magnetic relaxation time $\tau_{Dy}$, where $1/\tau_{Dy}$ is the frequency of the maximum in $\chi''(f)$ at a given temperature.[48,49] Figure 5(f) shows $\tau_{Dy}(T)$. Points are not shown for temperatures where $\chi''(f)$ did not show a maximum in our frequency range (0.1–500 Hz). The relaxation time $\tau_{Dy}$ clearly increases with decreasing temperature, with $\tau_{Dy} \sim 1$ s at $T = 3.0$ K, and $\tau_{Dy} \gtrsim 10$ s can be inferred for temperatures lower than 2.9 K. The slow time scale of magnetization relaxation in $DyScO_3$ is consistent with a previous report of a spin ice-like spin freezing with onset at $T \sim 25$ K,[28] and gives a good agreement with the slow relaxation of angular magnetoresistance observed in epitaxial $Sr_{1-x}La_xCuO_2$ films [Figs. 5 (a)–5(d)].

Our observation of positive magnetoresistance is different from previous reports of negative magnetoresistance in $Sr_{1-x}La_xCuO_2$ films grown on non-magnetic $KTaO_3$,[36] which was more than one order of magnitude smaller and had an onset at temperatures of a few tenths of Kelvin. Our measurement accuracy and limitation to fields below 10 kOe may not be sufficient to discern such contribution. The magnitude of the low-temperature positive magnetoresistance is comparable to that in 3d transition-metal alloys or oxides (0.1%–0.5%).[50–53] We attribute the positive magnetoresistance and anisotropic magnetoresistance observed in field sweeps in Figs. 2(a) and 3(b) to static magnetostriction of the substrate. It is known that strain from the substrate sensitively affects the resistivity of $Sr_{1-x}La_xCuO_2$ films. Tensile strain on $KTaO_3$ (100) substrates ($a_0 = 3.989$ Å) and compressive strain on Sr $TiO_3$ (100) substrates ($a_0 = 3.905$ Å) lead to a severalfold increase in resistivity and a decreased $T_c$, and even semiconducting $\rho$–$T$ curves.[14,21] The increase in magnetoresistance for fields along [−110] direction [Fig. 3(b)] is consistent with larger magnetostriction in fields along [−110] direction [Fig. S1(c)]. Further, the sharp and hysteretic angular magnetoresistance in Fig. 4(c) is different from the smooth two- and four-fold angular magnetoresistance reported in $Sr_{1-x}La_xCuO_2$ films on $KTaO_3$ which was attributed to antiferromagnetism of the $CuO_2$ planes.[35,36] Based on the agreement with angular magnetostriction [Fig. 4(f)] and slow magnetization dynamics in $DyScO_3$ [Figs. 5(e)–5(f)], we propose that it reflects a coupling of charge in $Sr_{1-x}La_xCuO_2$ to magnetization relaxation processes in $DyScO_3$.

The angular magnetoresistance is qualitatively different above and below the metamagnetic transition [Fig. 4(a)]. For fields smaller than $H_s = 3$ kOe, moments largely keep an antiparallel alignment in the *ab* plane, while they undergo a small tilt into *c*-direction for the magnetic field along [001] direction which is responsible for the small magnetization measured along [001] direction [Fig. 1 (d)]. The latter is still true for fields larger than $H_s$ along [001] direction, but when applied along [−110], a spin flop transition likely takes place in the *ab* plane.[28] Similarly, angular change in magnetostriction only appears for fields larger than $H_s$ [Fig. 4(f) and Fig. S1(c)]. A metamagnetic transition occurring in $DyScO_3$ during rotation in magnetic fields larger than $H_s$ may be responsible for the qualitative difference in angular magnetoresistance below and above $H_s$. Notable is that for rotations close to [−110] (easy axis) direction, changes in magnetoresistance are much smaller than the abrupt peaks and dips observed for rotations close to [001] (hard axis) direction [Fig. 4(c)], which is consistent with broad magnetostriction maxima around [−110] [Fig. 4(f)]. This could be an


© 2022 The Japan Society of Applied Physics

indication of $DyScO_3$ magnetic moments being pushed into the configuration along the easy axis direction by magnetic anisotropy.[52)] More detailed experiments on magnetic properties in $DyScO_3$ such as magnetometry will be required to confirm such hypotheses.

Finally, we note that hysteretic magnetoresistance below 5 K was also reported in $SrIrO_3$ epitaxial films on $DyScO_3$ (110) substrates.[31)] In that case magnetic field was applied along [110] direction (out of plane), and large spin polarization of carriers in $SrIrO_3$ along $DyScO_3$ easy axis was thought to affect spin-flip scattering and cause a difference in magnetoresistance along [001] and [1-10] directions. The magnetic order in $DyScO_3$ may be providing a playground for various substrate-induced transport phenomena in epitaxial thin films.

In summary, we have measured the magnetoresistance of epitaxial thin film $Sr_{1-x}La_xCuO_2$ grown by molecular beam epitaxy on $DyScO_3$ (110) substrates, and we have found anisotropic magnetoresistance and hysteretic angular magnetoresistance at low temperatures, strongly correlated with the Néel transition and the magnetocrystalline anisotropy in $DyScO_3$. Such magnetoresistance features were not observed in polycrystalline Cu or Pt thin films on $DyScO_3$, suggesting stronger modulation of magnetotransport in epitaxial $Sr_{1-x}La_xCuO_2$. Our results may lead to further insights into the magnetotransport of epitaxial films grown on $DyScO_3$.

**Acknowledgments** We thank Leonid Rokhinson and Kim-Khuong Huynh for useful discussions. We acknowledge Tomoyuki Ogawa, Kesami Saito, Katsumi Nagase, AIMR Common Equipment Unit, and Tohoku University Technical Support Center for technical support. This research was partially supported by the Tohoku-Tsinghua Collaborative Research Fund, WPI-AIMR Fusion Research Program, Center for Science and Innovations in Spintronics, JSPS KAKENHI (No. 19K23414, No. 20K14397, No. 18H03858, and No. 21K18590), and the Asahi Glass Foundation.

1) T. Siegrist, S. M. Zahurak, D. W. Murphy, and R. S. Roth, Nature **334**, 231 (1988).
2) M. G. M. Smith, A. Manthiram, J. Zhou, J. B. Goodenough, and J. T. Markert, Nature **351**, 549 (1991).
3) S. Ishiwata, D. Kotajima, N. Takeshita, C. Terakura, S. Seki, and Y. Tokura, J. Phys. Soc. Jpn. **82**, 063705 (2013).
4) C.-T. Chen, P. Seneor, N.-C. Yeh, R. P. Vasquez, L. D. Bell, C. U. Jung, J. Y. Kim, M.-S. Park, H.-J. Kim, and S.-I. Lee, Phys. Rev. Lett. **88**, 227002 (2002).
5) J. W. Harter, L. Maritato, D. E. Shai, E. J. Monkman, Y. Nie, D. G. Schlom, and K. M. Shen, Phys. Rev. Lett. **109**, 267001 (2012).
6) C. U. Jung, J. Y. Kim, M.-S. Kim, M.-S. Park, H.-J. Kim, Y. Yao, S. Y. Lee, and S.-I. Lee, Physica C **366**, 299 (2002).
7) R.-F. Wang, J. Guan, Y.-L. Xiong, X.-F. Zhang, J.-Q. Fan, J. Zhu, C.-L. Song, X.-C. Ma, and Q.-K. Xue, Phys. Rev. B **102**, 100508(R) (2020).
8) Y. Zhong et al., Phys. Rev. Lett. **125**, 077002 (2020).
9) Y. Zhong et al., Phys. Rev. B **97**, 245420 (2018).
10) M. A. Kastner, R. J. Birgeneau, G. Shirane, and Y. Endoh, Rev. Mod. Phys. **70**, 897 (1998).
11) J. D. Jorgensen, P. G. Radaelli, D. G. Hinks, J. L. Wagner, S. Kikkawa, G. Er, and F. Kanamaru, Phys. Rev. B **47**, 14654(R) (1993).
12) G. Er, Y. Miyamoto, F. Kanamaru, and S. Kikkawa, Physica C **181**, 206 (1991).
13) N. Ikeda, Z. Hiroi, M. Azuma, M. Takano, Y. Bando, and Y. Takeda, Physica C **210**, 367 (1993).
14) S. Karimoto, K. Ueda, M. Naito, and T. Imai, Appl. Phys. Lett. **79**, 2767 (2001).
15) V. Leca, D. H. A. Blank, G. Rijnders, S. Bals, and G. van Tendeloo, Appl. Phys. Lett. **89**, 092504 (2006).
16) Z. Z. Li, I. Matei, and H. Raffy, Physica C Supercond **460**, 452 (2007).
17) L. Maritato, A. Galdi, P. Orgiani, J. W. Harter, J. Schubert, K. M. Shen, and D. G. Schlom, J. Appl. Phys. **113**, 053911 (2013).
18) M. Liang, M. N. Kunchur, L. Fruchter, and Z. Z. Li, Physica C **492**, 178 (2013).
19) V. Jovanovic, Z. Z. Li, F. Bouquet, and H. Raffy, J. Phys.: Conf. Ser. **150**, 052086 (2009).
20) V. P. Jovanovic, Z. Z. Li, and H. Raffy, Supercond. Sci. Technol **24**, 055002 (2011).
21) S. Karimoto and M. Naito, Appl. Phys. Lett. **84**, 2136 (2004).
22) K. J. Choi et al., Science **306**, 1005 (2004).
23) J. H. Haeni et al., Nature **430**, 758 (2004).
24) Z. Y. Zhai, X. S. Wu, H. L. Cai, X. M. Lu, J. H. Hao, J. Gao, W. S. Tan, Q. J. Jia, H. H. Wang, and Y. Z. Wang, J. Phys. D: Appl. Phys. **42**, 105307 (2009).
25) M. Raekers et al., Phys. Rev. B **79**, 125114 (2009).
26) M. Bluschke, A. Frano, E. Schierle, M. Minola, M. Hepting, G. Christiani, G. Logvenov, E. Weschke, E. Benckiser, and B. Keimer, Phys. Rev. Lett. **118**, 207203 (2017).
27) Y.-D. Wu, Y.-L. Qin, X.-H. Ma, R.-W. Li, Y.-Y. Ei, and Z.-F. Zi, J. All. Com. **777**, 673 (2019).
28) X. Ke, D. G. Schlom, M. Bernhagen, R. Uecker, and P. Schiffer, Appl. Phys. Lett. **94**, 152503 (2009).
29) S. M. Wu, J. E. Pearson, and A. Bhattacharya, Phys. Rev. Lett. **114**, 186602 (2015).
30) L. S. Wu et al., Phys. Rev. B **96**, 144407 (2017).
31) A. K. Jaiswal, A. G. Zaitsev, R. Singh, R. Schneider, and D. Fuchs, AIP Adv. **9**, 125034 (2019).
32) I. Zutic, J. Fabian, and S. Das Sarma, Rev. Mod. Phys. **76**, 323 (2004).
33) J. Linder and J. W. A. Robinson, Nat. Phys. **11**, 307 (2015).
34) W. Han, S. Maekawa, and X.-C. Xie, Nat Mater **19**, 139 (2019).
35) V. P. Jovanovic, H. Raffy, Z. Z. Li, G. Remenyi, and P. Monceau, Phys. Rev. B **103**, 014520 (2021).
36) V. P. Jovanovic, L. Fruchter, Z. Z. Li, and H. Raffy, Phys. Rev. B **81**, 134520 (2010).
37) D. L. Miller, M. W. Keller, J. M. Shaw, K. P. Rice, R. R. Keller, and K. M. Diederichsen, AIP Adv. **3**, 082105 (2013).
38) S. Lee et al., Sci. Rep. **4**, 6230 (2014).
39) N. Nakamura, Y. Kake, H. Ogi, and M. Hirao, J. Appl. Phys. **108**, 043525 (2010).
40) J. Lustikova, Y. Shiomi, Z. Qiu, T. Kikkawa, R. Iguchi, K. Uchida, and E. Saitoh, J. Appl. Phys. **116**, 153902 (2014).
41) S. Karimoto, K. Ueda, M. Naito, and T. Imai, Physica C **378**, 127 (2002).
42) S. Karimoto and M. Naito, Physica C **412**, 1349 (2004).
43) H. Nakayama et al., Phys. Rev. Lett. **110**, 206601 (2013).
44) N. P. Kolmakova and I. B. Krynetskii, J. Magn. Magn. Mater. **130**, 313 (1994).
45) A. M. Kadomtseva, I. B. Krynetsky, M. D. Kuz'min, and A. K. Zvezdin, J. Magn. Magn. Mater. **81**, 196 (1989).
46) A. A. Minakov, I. V. Shvets, and V. G. Veselago, J. Magn. Magn. Mater. **88**, 121 (1990).
47) Y. Kota, E. Niwa, and M. Naoe, J. Appl. Phys. **129**, 203901 (2021).
48) J. Snyder, B. G. Ueland, A. Mizel, J. S. Slusky, H. Karunadasa, R. J. Cava, and P. Schiffer, Phys. Rev. B **70**, 184431 (2004).
49) C. V. Topping and S. J. Blundell, J. Phys.: Cond. Matter. **31**, 013001 (2019).
50) R. Galceran et al., Sci. Rep. **6**, 35471 (2016).
51) D. Kriegner et al., Nat. Commun. **7**, 11623 (2016).
52) D. Kriegner et al., Phys. Rev. B **96**, 214418 (2017).
53) C. Wang, H. Seinige, G. Cao, J.-S. Zhou, J. B. Goodenough, and M. Tsoi, Phys. Rev. X **4**, 041034 (2014).


© 2022 The Japan Society of Applied Physics